Fractal Analysis of Weld Defect Patterns Obtained by Radiographic Tests

Juliano A. Tesser*, Ricardo T. Lopes*, André P. Vieira†, Lindberg L. Gonçalves† and João Marcos A. Rebello**

*Department of Nuclear Engineering, Federal University of Rio de Janeiro, RJ, Brazil
†Department of Metallurgical and Materials Engineering, Federal University of Ceará, CE, Brazil
**Department of Metallurgical and Materials Engineering, Federal University of Rio de Janeiro, RJ, Brazil

Abstract. This paper presents a fractal analysis of radiographic patterns obtained from specimens with three types of inserted welding defects: lack of fusion, lack of penetration, and porosity. The study focused on patterns of carbon steel beads from radiographs of the International Institute of Welding (IIW). The radiographs were scanned using a greyscale with 256 levels, and the fractal features of the surfaces constructed from the radiographic images were characterized by means of Hurst, detrended-fluctuation, and minimal-cover analyses. A Karhunen-Loève transformation was then used to classify the curves obtained from the fractal analyses of the various images, and a study of the classification errors was performed. The obtained results indicate that fractal analyses can be an effective additional tool for pattern recognition of weld defects in radiographic tests.

1. INTRODUCTION

In a recent paper, Silva *et al.* [1] discussed the characterization of failure mechanisms that occur in fiberglass-reinforced polymeric matrix composites when subjected to tensile and flexural loads. The characterization was based on the analysis of acoustic-emission signals emitted by the composite during the process of failure. By looking at some fractal properties of the acoustic emission signals, namely, the fractal indices related to the Hurst analysis [2], detrended-fluctuation analysis [3], minimal cover analysis [4], and the box-counting dimension analysis [5], they were able to distinguish the different failure modes.

The study presented in this paper aims to characterize, through fractal analyses, the welding defects present in radiographic images. We focused on patterns of carbon steel beads from radiographs of the International Institute of Welding (IIW). The images were scanned in 8-bit resolution (256 levels of grey), and then processed by using the software Image Pro Plus 4.0. In order to improve contrast, a median type filter was used to smooth unpredicted noise. From the scanned images, we built surfaces by associating the grey level at each pixel with a height variable. The patterns in each surface were then studied by fractal analyses.

In order to establish the parameters to be calculated, we first present a brief review of the numerical analysis used in the treatment of the data. Afterwards, we present and discuss the results obtained.
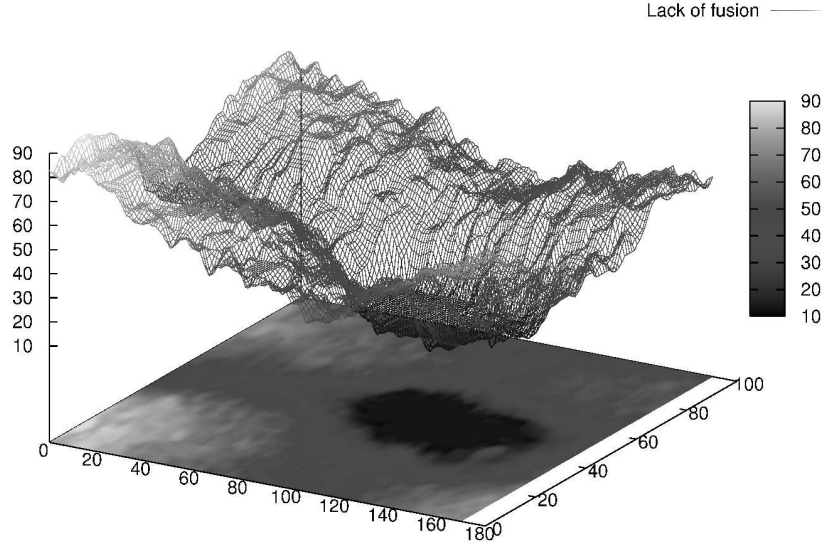
FIGURE 1. The bottom shows a radiographic image of a defect (lack of fusion), and above it is the corresponding surface, obtained by converting the greyscale to height variables.

2. FRACTAL ANALYSES

The numerical treatment of the images was performed on data generated from the 8-bit scanning of the radiographs, corresponding to 256 levels of grey, which are translated into a height variable z_{ij}. Here, (i, j) represents the coordinates of a pixel, with $i = 1$, 2, ..., L_x and $j = 1$, 2, ..., L_y for an image containing $L_x \times L_y$ pixels. This process is illustrated in Fig. 1

In the fractal analyses we considered extended two-dimensional versions of the Hurst (or R/S) analysis [2], detrended-fluctuation analysis (DFA) [3], and minimal-cover analysis [4]. In order to make the paper self-contained, we will present the details of the numerical techniques used in the analysis of the surfaces associated with the images, but first we make a few remarks that are generally valid.

All techniques start by covering the image with a grid composed of square cells containing $\tau \times \tau$ pixels, making sure that the grid is centered in both directions. This guarantees that, if L_x or L_y are not multiples of τ, only pixels in the periphery of the image are left outside the grid. Each technique then involves the calculation of the average of some quantity $Q(\tau)$ over all cells, for different values of τ. In a surface with genuine fractal features, $Q(\tau)$ should scale as a power of τ for $\tau \gg 1$,

$$Q(\tau) \sim \tau^{\eta}.$$

Fractals of different nature should give rise to different exponents η, providing a signature of the fractal. In our case, due to the finite amount of pixels and the limited resolution of the heights z_{ij}, this power-law behavior is hard to observe. However, as

discussed in the final section, we can still use the τ-dependence of the functions $Q(\tau)$ to characterize the different defects.

2.1. Hurst analysis

The rescaled-range (R/S) analysis was introduced by Hurst [2] as a tool for evaluating the persistency or antipersistency of a time series. The method works by dividing the series into a series of intervals, and calculating the average ratio of the range (the difference between the maximum and minimum values of the series) to the standard deviation inside each interval. The size of each interval is then varied.

We define a two-dimensional version of the R/S analysis in the following way. Given a $\tau \times \tau$ cell, whose lower left corner is located at pixel (i_0, j_0), we calculate $\langle z \rangle_\tau$, the average of z_{ij} inside the cell,

$$\langle z \rangle_\tau = \frac{1}{\tau^2} \sum_{(i,j)}' z_{ij} = \frac{1}{\tau^2} \sum_{i=i_0}^{i_0+\tau-1} \sum_{j=j_0}^{j_0+\tau-1} z_{ij}, \tag{1}$$

where the primed summation runs over all pixels (i, j) inside the cell. We then define an accumulated deviation from the mean as

$$Z_{ij} = \sum_{k=i_0}^{i} \sum_{l=j_0}^{j} \left(z_{kl} - \langle z \rangle_\tau \right), \tag{2}$$

from which we extract a range,

$$R(\tau) = \max_{\substack{i_0 \leqslant i \leqslant i_0+\tau-1 \\ j_0 \leqslant j \leqslant j_0+\tau-1}} Z_{ij} - \min_{\substack{i_0 \leqslant i \leqslant i_0+\tau-1 \\ j_0 \leqslant j \leqslant j_0+\tau-1}} Z_{ij} \tag{3}$$

and the corresponding standard deviation,

$$S(\tau) = \sqrt{\frac{1}{\tau} \sum_{(i.j)}' Z_{ij}^2}. \tag{4}$$

Finally, we obtain the rescaled range $R(\tau)/S(\tau)$, and take its average over all cells.

In a surface with true fractal features, the rescaled range should satisfy the scaling form

$$\frac{R(\tau)}{S(\tau)} \sim \tau^H, \tag{5}$$

where H is the Hurst exponent.

A typical curve obtained from the R/S analysis of the surfaces is shown in Fig. 2(a).

2.2. Detrended-fluctuation analysis

The detrended-fluctuation analysis (DFA) [3] aims to improve the evaluation of correlations in a time series by eliminating trends in the data.
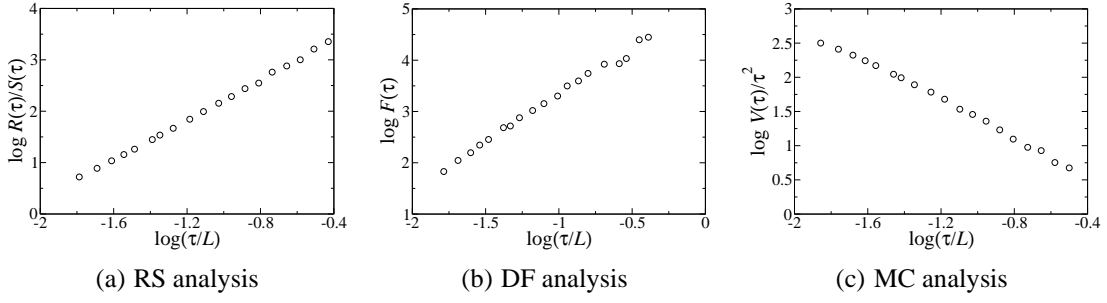
FIGURE 2. Typical curves obtained from the fractal analyses. The quantity L is defined as $L = \sqrt{L_x L_y}$.

Our two-dimensional extension of the method consists initially in obtaining a new integrated two-dimensional data set $\tilde{z}_{ij}$,

$$\tilde{z}_{ij} = \sum_{k=1}^{i} \sum_{l=1}^{j} (z_{kl} - \langle z \rangle), \qquad (6)$$

where the average $\langle z \rangle$ is taken over all pixels,

$$\langle z \rangle = \frac{1}{L_x L_y} \sum_{i=1}^{L_x} \sum_{j=1}^{L_y} z_{ij}. \qquad (7)$$

After building the grid (with cells of side τ), the integrated data inside a given cell is fitted by a plane. Then, a detrended variation function Δ_{ij} is obtained by subtracting from the integrated data the local trend as given by the fit. Explicitly, we define

$$\Delta_{ij} = \tilde{z}_{ij} - h_{ij}, \qquad (8)$$

where h_{ij} is the height associated with pixel (i, j) according to the fit. Finally, we calculate the root mean-square fluctuation $F(\tau)$ inside a cell as

$$F(\tau) = \sqrt{\frac{1}{\tau^2} {\sum_{(i,j)}}' \Delta_{ij}^2}, \qquad (9)$$

and average over all cells. For a true fractal surface, $F(\tau)$ should behave as

$$F(\tau) \sim \tau^{\alpha}, \qquad (10)$$

where α is the scaling exponent.

A typical curve obtained from the detrented-fluctuation analysis of the surfaces is shown in Fig. 2(b).

2.3. Minimal-cover analysis

This method has been recently introduced [4], and, in its original version, it relates the minimal area necessary to cover a given plane curve, at a specified scale, to a power-law behavior.

In our two-dimensional extension, the method relates the minimal volume necessary to cover a given surface, at a specified scale. After building the grid, we can associate with each $\tau \times \tau$ cell, labeled by a variable k, a prism of height A_k, defined as the difference between the maximum and minimum values of z_{ij} inside cell k,

$$A_k = \max_{\substack{i_0 \leqslant i \leqslant i_0 + \tau - 1 \\ j_0 \leqslant j \leqslant j_0 + \tau - 1}} z_{ij} - \min_{\substack{i_0 \leqslant i \leqslant i_0 + \tau - 1 \\ j_0 \leqslant j \leqslant j_0 + \tau - 1}} z_{ij}. \tag{11}$$

The minimal volume is then given by

$$V(\tau) = \sum_k A_k \tau^2, \tag{12}$$

where the summation runs over all cells.

Ideally, in the scaling region ($\tau \gg 1$), $V(\tau)$ should behave as

$$V(\tau) \sim \tau^{3 - D_\mu}, \tag{13}$$

where D_μ is the minimal cover dimension, which is equal to 2 when the surface presents no fractality.

A typical curve obtained from the minimal-cover analysis of the surfaces is shown in Fig. 2(c).

3. RESULTS AND DISCUSSION

In order to classify the images, we used a supervised variation of the Karhunen-Loève (KL) transformation [6], and applied it to the set of curves produced by the fractal analyses described in the previous Section. In this sense, the fractal analyses can be seen as a sophisticated preprocessing tool. For each image, we collected the corresponding curves from the three fractal analyses, forming a single vector with M components ($M = 57$).

We proceeded by first randomly dividing the vectors into a training set (with $N = 120$ vectors) and a test set (with 31 vectors), performing all the relevant operations (as described below), and calculating the confusion tables. Finally, we took averages over 300 different choices of training and test sets.

Let $\mathbf{x}_i$ be the vector corresponding to the ith image. The KL transformation consists of first projecting the training vectors along the eigenvectors of the within-class covariance matrix $\mathbf{S}_W$, defined by

$$\mathbf{S}_W = \frac{1}{N} \sum_{k=1}^{N_C} \sum_{i=1}^{N_k} y_{ik} (\mathbf{x}_i - \mathbf{m}_k)(\mathbf{x}_i - \mathbf{m}_k)^T, \tag{14}$$

TABLE 1. Average confusion matrix for the training vectors. The possible classes are lack of fusion (LF), lack of penetration (LP), porosity (PO) and no defects (ND). The figures in parenthesis indicate the standard deviations, calculated over 300 sets. The value in row i, column j indicates the percentage of vectors belonging to class i which were associated with class j.

	LF	LP	PO	ND
LF	87.4 (4.8)	7.5 (3.6)	4.9 (4.3)	0.2 (0.9)
LP	1.5 (2.1)	93.8 (3.4)	2.1 (2.6)	2.5 (2.4)
PO	0.2 (1.0)	1.4 (2.7)	97.0 (3.8)	1.4 (2.6)
ND	1.3 (1.2)	3.7 (1.8)	1.6 (1.1)	93.4 (2.3)

where $N_C = 4$ is the number of different classes, N_k is the number of vectors in class k, $\mathbf{m}_k$ is the average vector of class k, and T denotes the transpose of a matrix (in this case, of a column vector). The element y_{ik} is equal to one if $\mathbf{x}_i$ belongs to class k, and zero otherwise. We also rescale the resulting vectors by a diagonal matrix built from the eigenvalues λ_j of $\mathbf{S}_W$. In matrix notation, this operation can be written as

$$\mathbf{X}' = \Lambda^{-\frac{1}{2}}\mathbf{U}^T\mathbf{X}, \tag{15}$$

where $\mathbf{X}$ is the matrix whose columns are the training vectors $\mathbf{x}_i$, $\Lambda = \mathrm{diag}(\lambda_1, \lambda_2, ...)$, and $\mathbf{U}$ is the matrix whose columns are the eigenvectors of $\mathbf{S}_W$. This choice of coordinates makes sure that the transformed within-class covariance matrix corresponds to the unit matrix. Finally, in order to compress the class information, we project the resulting vectors onto the eigenvectors of the between-class covariance matrix $\mathbf{S}_B$,

$$\mathbf{S}_B = \sum_{k=1}^{N_C} \frac{N_k}{N}(\mathbf{m}_k - \mathbf{m})(\mathbf{m}_k - \mathbf{m})^T, \tag{16}$$

where $\mathbf{m}$ is the overall average vector. The full transformation can be written as

$$\mathbf{X}'' = \mathbf{V}^T\Lambda^{-\frac{1}{2}}\mathbf{U}^T\mathbf{X}, \tag{17}$$

where $\mathbf{V}$ is the matrix whose columns are the eigenvectors of $\mathbf{S}_B$ (calculated from $\mathbf{X}'$).

With 4 possible classes, the fully-transformed vectors have $4 - 1 = 3$ relevant components [6]. A vector $\mathbf{x}_i$ is associated with the class whose average vector lies closer to $\mathbf{x}_i$ within the transformed three-dimensional space.

After using the training vectors to obtain the full transformation, the classification can be checked with those same vectors. The resulting average confusion matrix is displayed in Table 1. When employed to classify the testing vectors, the KL transformation produces the confusion matrix shown in Table 2. From the tables we can see that the training vectors are associated with the correct class in about 90% of the cases, whereas the percentage of correct classification for the testing vectors is about 50%. This last result surely lies above the expected rate produced by random association (which would be 25% in this case).

TABLE 2. The same as in Table 1, for the testing vectors.

	LF	LP	PO	ND
LF	48.1 (23.6)	19.8 (20.7)	22.8 (19.9)	9.2 (14.7)
LP	10.7 (11.9)	55.1 (18.8)	14.3 (14.0)	19.9 (16.1)
PO	12.2 (16.3)	14.7 (18.6)	57.6 (25.0)	15.5 (19.1)
ND	9.4 (8.7)	19.2 (11.2)	13.7 (10.1)	57.6 (14.3)

In summary, we have shown that fractal analyses are a promising tool for classifying welding defects in radiographic images. We believe that its efficiency can be considerably improved by using a larger sample of images, as well as by working with 16-bit scans, which would greatly enhance the grey-level resolution. We are currently working on this direction.

ACKNOWLEDGMENTS

REFERENCES

1. F. E. Silva, L. L. Gonçalves, D. B. B. Fereira, and J. M. A. Rebello, *Chaos, Solitons & Fractals* **26**, 481–494 (2005).
2. H. E. Hurst, *Trans. Am. Soc. Civ. Eng.* **116**, 770–808 (1951).
3. C. K. Peng, V. Buldyrev, S. Havlin, M. Simmons, H. R. Stanley, and A. L. Goldberger, *Phys. Rev. E* **49**, 1685–1689 (1994).
4. M. M. Dubovikov, N. V. Starchenko, and M. S. Dubovikov, *Physica A* **339**, 591–608 (2004).
5. P. S. Addison, *Fractals and Chaos*, IOP, London, 1997.
6. A. R. Webb, *Statistical Pattern Recognition*, John Wiley & Sons, West Sussex, 2002.